Polymer 50 (2009) 2885–2892

Contents lists available at ScienceDirect

Polymer

journal homepage: www.elsevier.com/locate/polymer

Hydrogen bonding interactions and miscibility studies of poly(amide)/poly-(vinyl pyrrolidone) blends containing mangiferin

Chandrasekaran Neelakandan, Thein Kyu*

Department of Polymer Engineering, University of Akron, Akron, OH 44325, USA

ARTICLE INFO

Article history:
Received 6 March 2009
Received in revised form
23 April 2009
Accepted 25 April 2009
Available online 3 May 2009

Keywords:
Hydrogen bonding
Morphology phase diagram
Polymer blends

ABSTRACT

Miscibility studies of amorphous poly(amide)/poly(vinyl pyrrolidone) (PA/PVP) blends containing a crystalline phytochemical called "mangiferin" have been carried out using differential scanning calorimetry, Fourier transformed infrared spectroscopy and polarized optical microscopy. The binary blends of PA/PVP prepared from dimethylsulfoxide solutions were found to be completely miscible showing a systematic movement of a single glass transition temperature over the entire composition range. The FTIR study indicated the occurrence of cross-hydrogen bonding interactions between PA and PVP, which may be responsible for complete miscibility of the PA/PVP pair. Moreover, cross-hydrogen bonding promotes miscibility in binary blends of PA/mangiferin and PVP/mangiferin. However, the addition of mangiferin to PA/PVP blends has resulted in liquid–liquid phase separation between PA/mangiferin and PVP/mangiferin phases due to the preferential affinity of mangiferin to PVP than to PA. With increasing mangiferin concentration, liquid–liquid phase segregations occur between PA + mangiferin and PVP + mangiferin phases in addition to the solid–liquid phase transition of mangiferin crystals. Lastly, a ternary morphology phase diagram of the PA/PVP/mangiferin blends was established, which exhibited various coexistence regions such as isotropic, liquid + liquid, liquid + crystal, liquid + liquid + crystal, and solid crystal regions.

1. Introduction

Past couple of decades has witnessed a tremendous surge in interest on plant-derived, non-nutritive compounds called phytochemicals owing to their multi biomedical properties including anti-oxidant, anti-inflammation, anti-tumor, and anti-microbial properties [1–3]. Phytochemicals have been under extensive investigation as potential compounds for treatment of major diseases such as diabetes, cardiovascular disease, cancer, and hypertension [4]. Some of the compelling advantages of using phytochemicals include their natural origin in plants, fruits and vegetables, abundant availability, easy extraction, minimal levels of toxicity, and inexpensiveness compared to their synthetic counterparts [5,6].

Recently, there has been a paradigm shift in biomaterials research from "inert" biomaterials (first generation) to "bioactive" materials (second generation) to materials that stimulate specific cellular responses at a molecular level (third generation) [7]. There is also a strong need to reduce infection, which may be realized through anti-microbial surface treatments, non-fouling surface and anti-biotic controlled surface release [8]. In other words, there is an imminent and strong need for multifunctional biomaterials. In this regards, a simple and an effective approach has been sought to form multifunctional biomaterials by utilizing polymer/phytochemical blends, which also fits perfectly within this scope of development of third generation biomaterials.

The ultimate goal of the present study is to develop multifunctional hemodialyzer (HD) membranes by incorporating phytochemicals such as mangiferin into polymer blends [9,10]. Mangiferin is a naturally occurring glucosyl xanthone (2-C-β-D-glucopyranosyl-1,3,6,7-tetrahydroxyxanthone) derived from barks and leaves of a mango tree (*Mangifera indica*). It is a crystalline substance having a molecular weight of 422 g/mol and a melting temperature of ~267 °C. It is well known for its anti-oxidant [11–16], anti-tumor [17], anti-viral [18–20] anti-bacterial and anti-fungal [21], immunomodulatory [22–24] and anti-diabetic [25,26] properties. Other important properties of mangiferin include anti-platelet [27], anti-thrombotic [28], and anti-inflammation [29]. These biological and pharmacological activities (hereafter called 'multifunctional properties' for brevity) of xanthone derivatives, specifically mangiferin, along with its isolation and characterization techniques are reported elsewhere [30–35]. By virtue of these important multi biomedical properties, it is our interest to incorporate mangiferin into HD membranes. However, prior to fabricating HD membranes modified with mangiferin, it is

* Corresponding author. Tel.: +1 330 972 6672; fax: +1 330 258 2339.
E-mail address: tkyu@uakron.edu (T. Kyu).

0032-3861/$ – see front matter © 2009 Elsevier Ltd. All rights reserved.
doi:10.1016/j.polymer.2009.04.054

crucial to understand molecular interactions of mangiferin with its polymer counterparts and their miscibility behavior.

The present article focuses primarily on the miscibility aspects of amorphous poly(amide)/poly(vinyl pyrrolidone) (PA/PVP) blends with and without mangiferin modifications. Miscibility behavior of binary blends of PA/PVP, PA/mangiferin, and PVP/mangiferin are characterized by differential scanning calorimetry (DSC) and subsequently by Fourier transformed infrared spectroscopy (FTIR) for determining specific inter-molecular interactions involving a competition between self-hydrogen bonding of PA and cross-hydrogen bonding between PA and PVP constituents, contributing to their blend miscibility [36–39]. Subsequently, this miscibility characterization approach has been extended to their ternary blends with emphasis on the relationship between the emerged phase morphologies and the ternary phase diagram.

2. Experimental section

2.1. Materials

In preparation of polymer/phytochemical blends, an amorphous PA/PVP pair was chosen as the polymer matrix and mangiferin, a crystalline compound, as the phytochemical. The amorphous polyamide (TROGAMID® T5000) was provided by Degussa Corporation (New Jersey, USA), having number-average and weight-average molecular weights of $M_n = 20{,}000$ and $M_w = 63{,}000$ [36], respectively. It has excellent film forming properties with reported water absorption of 5.1 wt% under specified conditions [37]. PVP ($M_w = 40{,}000$) was bought from Sigma–Aldrich, USA. A reagent grade dimethylsulfoxide (DMSO) was purchased from Sigma-Aldrich and utilized as received without further purification. This PA/PVP pair has been shown to be biocompatible and has been widely used as hemodialyzer membranes [40]. Mangiferin purchased from Sigma–Aldrich was of high performance liquid chromatography (HPLC) grade having 99.9% purity.

2.2. Methods

Thermal analysis of the samples was conducted at a heating rate of 10 °C/min using differential scanning calorimeter (DSC) (TA Instruments, Model 2920) calibrated for temperature and enthalpy using indium standard having a melting point of 165.5 °C. Thermal stability studies were conducted using a thermogravimetric analyzer (TGA) (TA Instruments, Model 2050). Approximately 10 mg of the samples were used for each run. As received PA, PVP, and mangiferin were subjected to TGA analysis from 25 °C to 500 °C at a heating rate of 10 °C/min in a nitrogen atmosphere at a flow rate of 120 mL/min. The TGA experiments were also performed on solvent cast samples. The temperature at which the weight loss of 5% occurred was regarded as the degradation temperature. For DSC experiments, solutions of neat PA, PVP, mangiferin and their blends were prepared in DMSO at a polymer concentration of 10 wt% and homogenized for 48 h followed by solvent casting under vacuum at 150 °C for 24 h. During the first DSC run, the samples were heated only up to 225 °C (owing to the thermal stability of mangiferin) to remove any thermal history followed by a second run in which the samples were heated up to 300 °C to cover the melting transition of the mangiferin.

Binary and ternary blends of PA/PVP with or without mangiferin were prepared by solution casting on KBr discs for infrared analyses from the 5 wt% polymer solution in DMSO. The samples were dried under vacuum at 150 °C for 24 h to ensure complete removal of any residual solvent. The samples were then stored in desiccators until further use. Infrared measurements were recorded on a FTIR spectrometer (Thermo Scientific Nicolet 380) at a resolution of 4 cm^{-1} averaged over 32 scans. Since each of the components show considerable affinity towards moisture, care was exercised to minimize the effects of moisture absorption. That is to say, the samples were heated to 150 °C in a controlled temperature cell attached to the FTIR spectrometer and equilibrated at 100 °C. The FTIR spectra were recorded at 100 °C such that the samples are free of moisture or residual solvent. The samples for POM experiments were prepared under the same conditions of DSC and FTIR, except that thin films (~10 μm) were cast directly on glass substrates. All samples were stored in a desiccator until further use. An optical microscope (BX60, Olympus) equipped with a 35 mm digital camera (EOS 400D, Canon) and a hot stage (TMS 93, Linkam) was used in the POM study.

3. Results and discussion

3.1. Thermal stability and miscibility characteristics of PA/PVP binary blends

Fig. 1(a) exhibits the chemical structures and TGA thermograms of neat PA and PVP indicating both polymers to be thermally stable up to ~350 °C. Visually, the solvent cast films of PA/PVP blends were transparent and colorless. In the DSC scans, a single T_g was found to shift systematically with blend composition (Fig. 1(b)). Moreover, the widths of these glass transition curves were comparable to those of pure components suggesting that the PA/

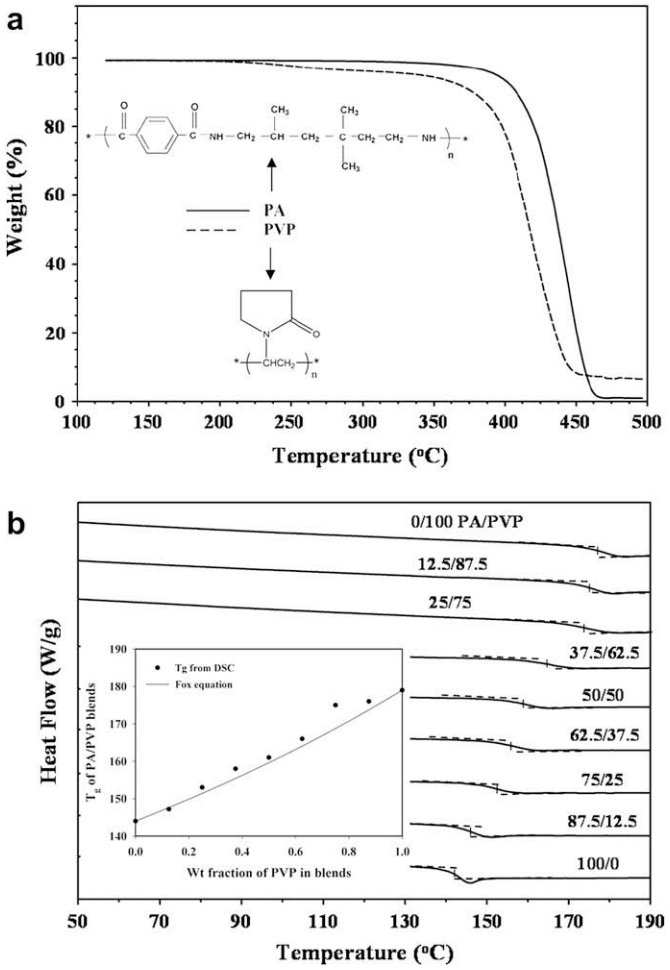

Fig. 1. (a) TGA thermograms of pure PA and PVP demonstrating the thermal stability of pure components. Insets show the chemical structures of the two polymers. (b) DSC thermograms of binary PA/PVP blends exhibiting a single T_g in all compositions. The dashed lines are used to identify the onset and the terminus of the glass transition. The midpoint of the transition is regarded as T_g.

PVP blends may be completely miscible over the entire composition range. In the comparison with the Fox equation [41], a positive departure was observed (see inset of Fig. 1(b)) implying possible occurrence of strong specific interactions between PA and PVP, which may be contributing to enhanced miscibility. The POM studies of PA/PVP blends revealed no evidence of any phase separated regions or crystalline textures, which are in good agreement with the DSC observation.

FTIR experiments were carried out in order to identify the source of this enhanced miscibility of the PA/PVP blends. Fig. 2(a) depicts the FTIR spectra of these PA/PVP blends in the 1550–1800 cm^{-1} range obtained at 100 °C. The 1640 cm^{-1} band of PA corresponds mostly to self-associated amide-I groups (i.e., hydrogen bonding within the same species) [38,39,42]. When PVP is added to PA, a new shoulder corresponding to free carbonyl group (C═O) appears in the 75/25 PA/PVP, which is probably released due to disruption of some of the self-associated amide-I bonds. Any further addition of PVP further causes the amide-I band to shift to a higher wavenumber implying the freeing up of more self-associated amide-I bonds due to disruption. A similar effect can be witnessed in the N–H stretching region (Fig. 2(b)), where some of the self-associated (intra-molecular hydrogen bonds) N–H vibrations are released, which causes the 3322 cm^{-1} band to shift to a higher wavenumber. While the released N–H groups should contribute to an increase in intensity of the free N–H band (3444 cm^{-1}), the trend shows an opposite trend. This seemingly inconsistent trend may be interpreted as a possibility that the released N–H groups probably undergo inter-molecular hydrogen bonding with the carbonyl groups of PVP. The net result is that the free N–H band shifts to a lower wavenumber despite marginally.

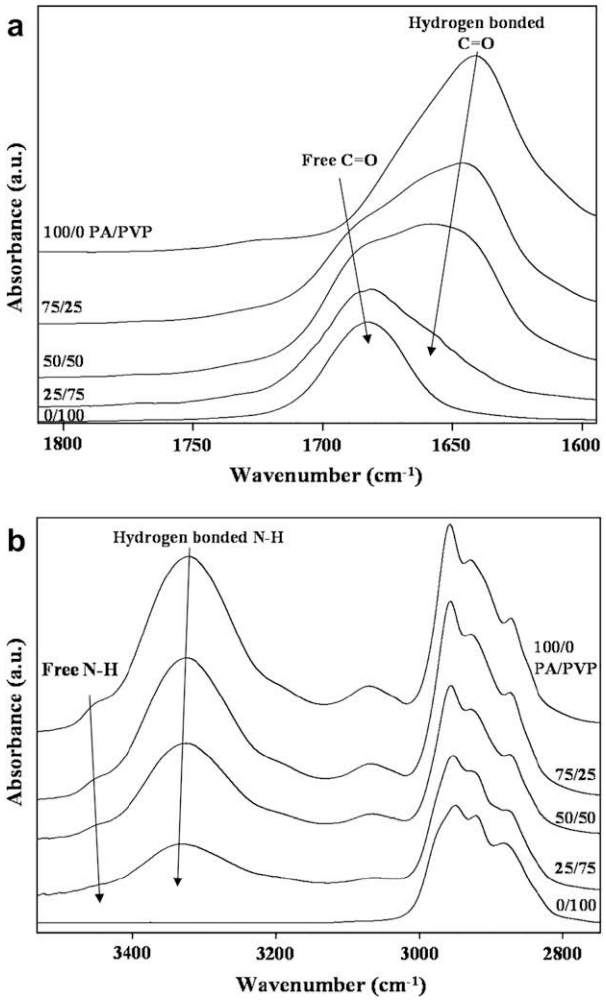

Fig. 2. FTIR spectra recorded at 100 °C for the PA/PVP blends (a) in the region of 1550–1800 cm^{-1} demonstrating cross-hydrogen bonding by the systematic movement of free carbonyl peak to lower wavenumbers (~8 cm^{-1}) and freeing up of hydrogen-bonded carbonyl groups shifting to higher wavenumbers (~17 cm^{-1}); and (b) in the 2750–3550 cm^{-1} range illustrating the release of some of the self-associated N–H groups of PA (~10 cm^{-1}) and formation of cross-hydrogen bonding of the free N–H of PA showing a blue shift (~15 cm^{-1}) upon addition of PVP.

It has been well documented that the PA molecules can self-associate and form self-hydrogen bonding within their own species; but PVP does not undergo self-hydrogen bonding, except that it can form cross-hydrogen bonding with the PA counterpart. Naturally, one can anticipate a competition between the disruption of self-hydrogen-bonded amide group of the PA molecules and the cross-hydrogen bonding between the N–H of PA and C═O of PVP. When the cross-hydrogen bonding is prevalent over that the self-hydrogen bonding of PA molecules, some of the self-associated PA groups must be disrupted, thereby freeing up some C═O and/or N–H bands resulting in the red shift. On the other hand, when the cross-hydrogen bonding occurs, the free amide groups interact with the carbonyl group of PVP and thus showing a spectral shift to a lower wavenumber. In high polymer blends, the entropic driving force is negligibly small, thus the miscibility will be dominated by the energetics of mixing. Hence, the cross-hydrogen bonding between PA and PVP must be stronger than that of the self-hydrogen bonding of PA in order to achieve the complete miscibility in the present PA/PVP system. Thus, the above FTIR result implies that the enhanced miscibility is due to stronger cross-hydrogen bonding between the N–H group of PA and the C═O group of PVP as compared to the self-hydrogen bonding among PA molecules.

3.2. Thermal stability of pure mangiferin and its PA binary blends

Fig. 3 exhibits the overlay of DSC and TGA thermograms of neat mangiferin along with its chemical structure. It can be clearly noticed that there is a significant weight loss of mangiferin that coincided with its crystal melting peak. It may be envisioned that the thermal stabilization of the mangiferin molecules can be improved through specific interactions such as cross-hydrogen bonding upon blending with its polymer counterparts.

The solvent cast PA/mangiferin samples were transparent to naked eyes, but tinted yellowish owing to the inherent color of mangiferin. As evidenced in Fig. 4(a), the degradation temperature of PA/mangiferin blends move up to elevated temperature with

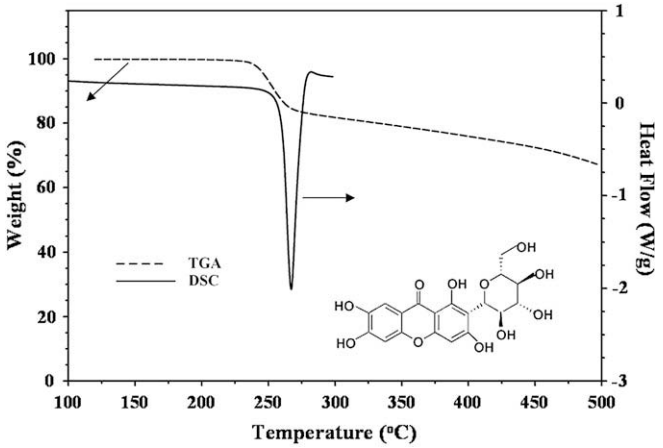

Fig. 3. Overlay of DSC and TGA thermograms for mangiferin illustrating the thermal decomposition of mangiferin occurring at its crystal melting point. The inset shows the chemical structure of mangiferin.

increasing PA loading. This improvement may be insignificant at low loading level (say 10 wt% of PA), but it becomes more pronounced with further increase of PA content. The DSC thermograms of PA/mangiferin are displayed in Fig. 4(b). A single T_g can be clearly discerned upon addition of mangiferin shifting systematically to higher temperatures. The increase in the T_g of the PA/mangiferin blends may be attributed to the rigidity of the heterocyclic backbone of mangiferin (i.e., xanthone in Fig. 3) and its polyphenolic nature containing numerous hydroxyl groups, which are capable of interacting with the amide groups of PA chains. The presence of crystal melting peak at higher mangiferin concentrations (>40 wt% of mangiferin) signifies the occurrence of liquid–solid phase transition and also underscores the solubility limit of mangiferin in PA. Another interesting feature of the DSC thermograms of the PA/mangiferin pair is the virtually invariant nature of the T_m of mangiferin (~267 °C) at low PA concentrations, but a slight depression of T_m occurs only when the PA concentration exceeded 50 wt%.

Fig. 5(a) exhibits the FTIR spectra of PA/mangiferin blends in the 1500–1800 cm^{-1} range. It should be emphasized that both PA and mangiferin are self-associating components, capable of forming intra-molecular hydrogen bonding. With the addition of mangiferin, it is seen that the amide-I band of PA exhibits a spectral shift (~8 cm^{-1}) to lower wavenumbers due to hydrogen bonding with hydroxyl groups of mangiferin. The C=O band of mangiferin shows a marginal shift to a lower wavenumber for about 4 cm^{-1}, suggesting a possibility of N–H···C=O interaction. In contrast, the aromatic C=C band does not show any movement since it is not involved in any specific interaction. It is more difficult to analyze band movements in the N–H stretching region due to the overlap of O–H and N–H stretching bands in some intermediate compositions. Nevertheless, the movement of the N–H band to the higher wavenumbers (Fig. 5(b)) is evident which may be attributed to the release of some of the hydrogen-bonded N–H groups of PA upon interacting with hydroxyl groups of mangiferin. On the same token, the amide-II band (1540 cm^{-1}) shifted to a lower wavenumber with mangiferin loading (~8 cm^{-1}), which is consistent for systems involving strong N–H···C=O interactions [43]. These observed spectral movements suggest the occurrence of hydrogen bonding between PA and mangiferin and possible interactions include N–H···C=O (self), N–H···C=O (cross), N–H···O–H (cross) and O–H···O–H (self) interactions.

3.3. Thermal and miscibility characteristics of PVP/mangiferin binary blends

Some similarities and differences can be noticed in the miscibility behaviors of the PA/mangiferin and PVP/mangiferin systems.

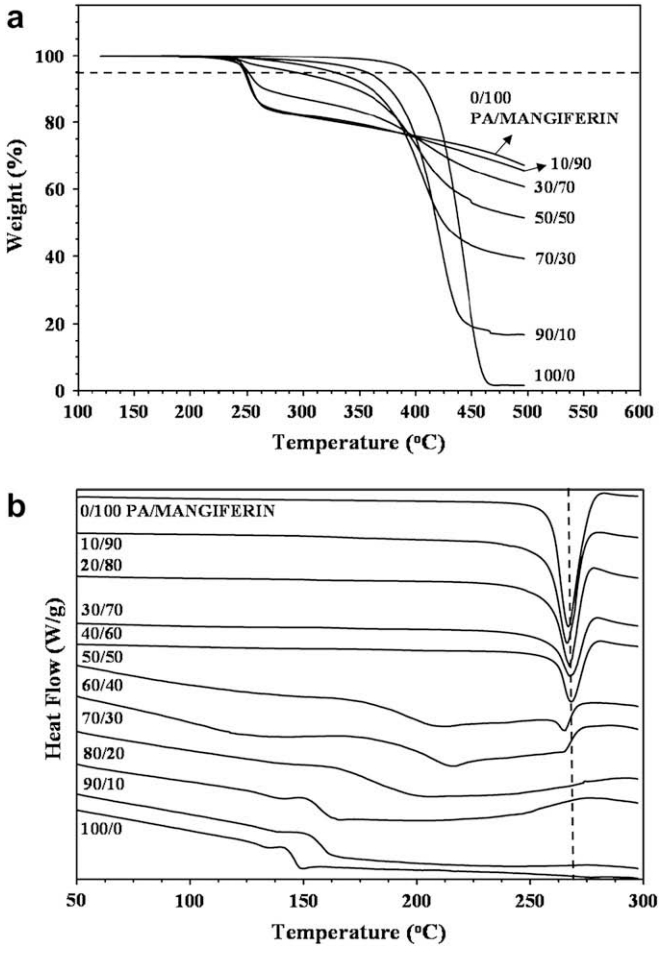

Fig. 4. (a) TGA thermograms for PA/mangiferin blends showing the improved thermal stability of mangiferin due to the addition of PA. The horizontal dashed line corresponds to the 5% weight loss. (b) Second run DSC thermograms for PA/mangiferin showing single T_g and its systematic movement to higher temperature at lower mangiferin concentrations, whereas an endothermic crystal melting peak at higher mangiferin concentrations.

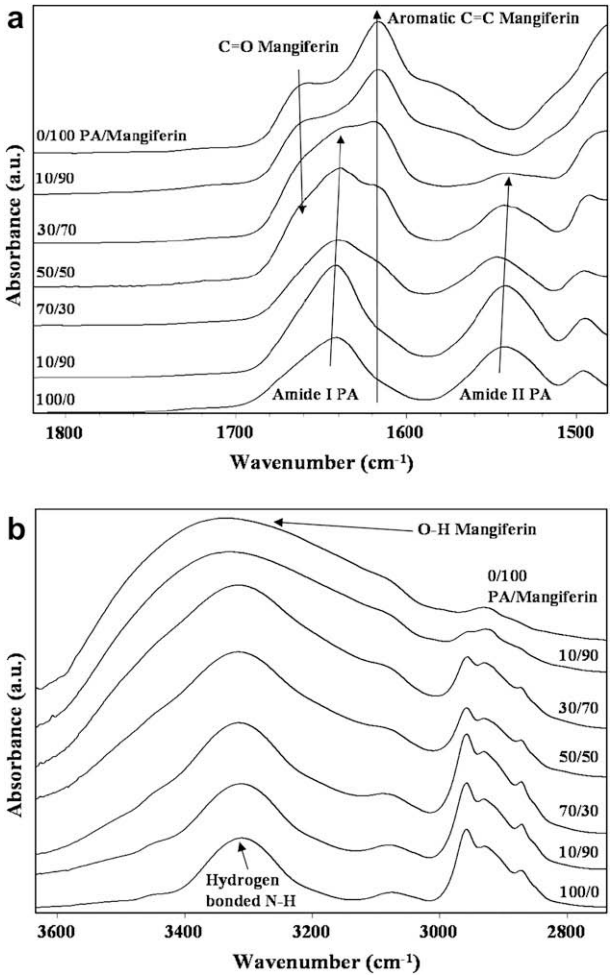

Fig. 5. FTIR spectra of the PA/mangiferin blends recorded at 100 °C: (a) in the range of 1500–1800 cm^{-1} showing the spectral shift of amide-I and amide-II bands of PA for ~8 cm^{-1} and carbonyl band of mangiferin to lower wavenumbers for ~4 cm^{-1} upon blending and (b) in the 2700–3600 cm^{-1} range for PA/mangiferin blends showing the spectral shift of O–H band of mangiferin with increasing PA. Note that the broad O–H band of mangiferin and the N–H of PA band can mutually interfere and thus the band shift was not quantified.

Visually, all PVP/mangiferin blends were transparent, but tinted yellowish. TGA thermograms of PVP/mangiferin blends (Fig. 6(a)) illustrate the improved thermal stability of mangiferin due to the addition of PVP. DSC thermograms of PVP/mangiferin samples also exhibited single T_g, which consistently moved to higher temperatures with increasing mangiferin concentration (Fig. 6(b)). No liquid–liquid phase separation was observed in the entire composition and temperature range investigated, but large spherulitic structures developed at higher mangiferin concentrations signifying the isotropic liquid + crystal coexistence regions. However, unlike PA/mangiferin blends, PVP/mangiferin blends showed isotropic-crystal transition at a much higher mangiferin composition (80 wt% vs. 30 wt%). One major difference between the PVP/mangiferin and PA/mangiferin systems is related to the depression of melting point of PVP/mangiferin blends, which is more significant as compared to PA/mangiferin blends. This observation combined with the larger isotropic composition range for PVP/mangiferin blends implies that mangiferin is more miscible with PVP than with PA. The reason for PVP to show preferential affinity towards mangiferin is probably due to strong interactions between PVP and glucose of mangiferin. The present finding is consistent with the literature reports demonstrating strong cross-hydrogen bonding interactions between PVP and various saccharide moieties [44–46].

It should be recalled that PVP does not self-associate, but it contains functional groups such as C═O groups that are capable of interacting with O–H groups of mangiferin via cross-hydrogen bonding interaction. Fig. 7 (a) and (b) illustrate the FTIR spectrum of PVP/mangiferin blends in the 1500–1800 and 2700–3600 cm^{-1} range, respectively. These spectra were acquired at 100 °C to minimize moisture absorption. Pure mangiferin shows a broad band at 3366 cm^{-1} corresponding to the O–H stretching, whereas PVP has no such peak in the corresponding region. The FTIR analysis of the present PVP/mangiferin system is relatively straightforward because only mangiferin can self-associate. The addition of PVP is expected to free up some of the self-associated hydroxyl groups of mangiferin due to cross-hydrogen bonding between C═O of PVP and O–H of mangiferin. The decreasing trend of the O–H stretching band of mangiferin with PVP loading seems to be governed by the competition between hydroxyl–hydroxyl (self-association) of mangiferin and hydroxyl–carbonyl (cross-hydrogen bonding) interactions between the constituents. As the concentration of PVP is increased the hydroxyl band becomes even broader and shifts to lower frequencies while reducing its magnitude. The corresponding effect can be explicitly seen in the carbonyl spectral region in which the carbonyl peak of PVP moves to lower frequencies due to strong

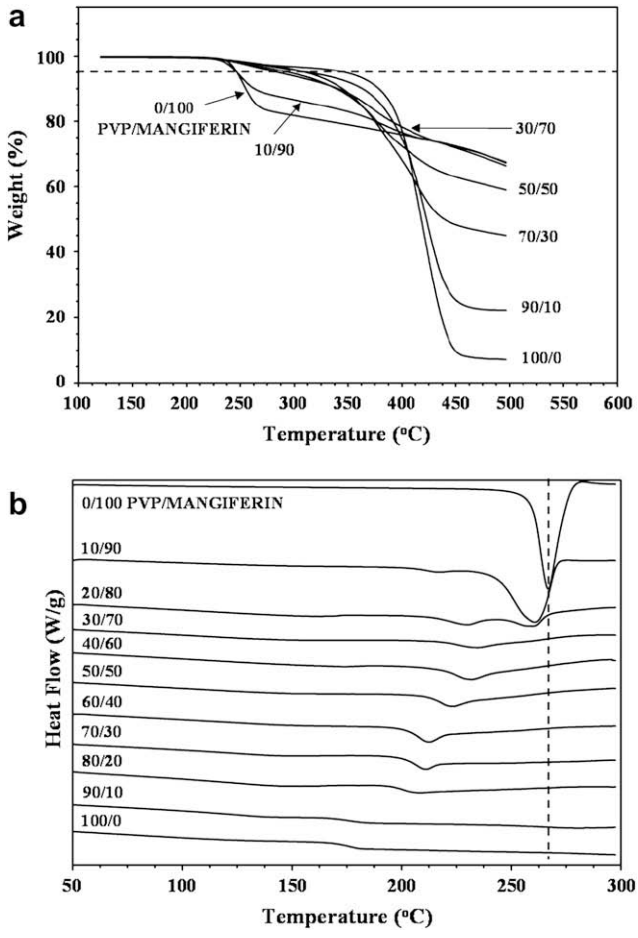

Fig. 6. (a) TGA thermograms of PVP/mangiferin blends showing improved thermal stability of mangiferin due to the addition of PVP. The horizontal dashed line corresponds to the 5% weight loss. (b) Second run DSC thermograms of PVP/mangiferin blends showing a similar trend as that of PA/mangiferin blends, but larger melting point depression suggesting greater miscibility of the PVP/mangiferin blends as compared with the PA/mangiferin blends.

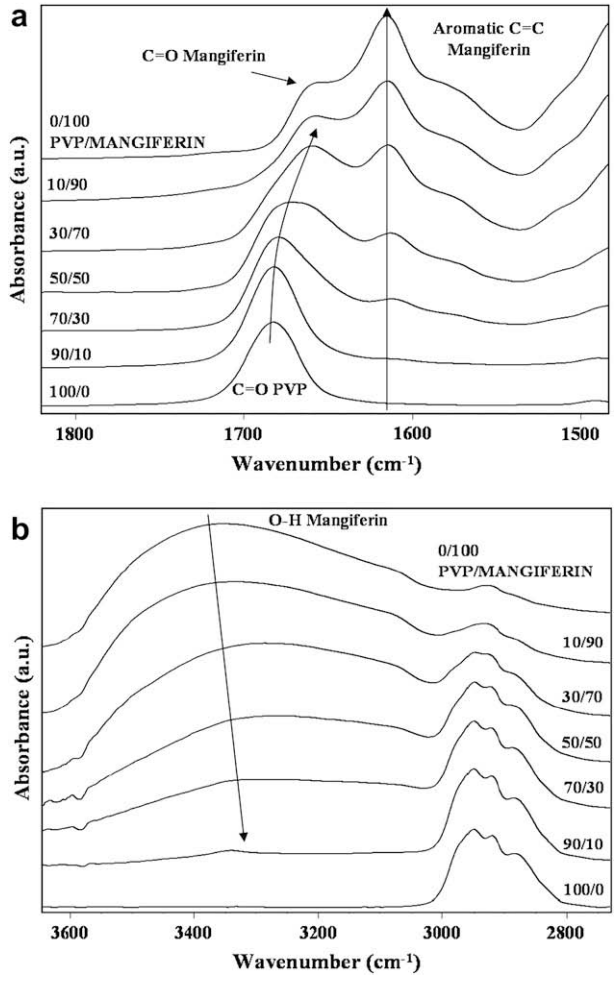

Fig. 7. FTIR spectra recorded at 100 °C (a) in the range 1500–1800 cm^{-1} for PVP/mangiferin blends demonstrating systematic movement of carbonyl bands of both PVP and mangiferin constituents (~25 cm^{-1}) in contrast to the stationary aromatic C═C band of mangiferin showing no spectral shift. (b) In the 2700–3600 cm^{-1} range the PVP/mangiferin blends show drastic shift of O–H band of mangiferin bands to lower wavenumbers (~90 cm^{-1}) suggesting cross-hydrogen bonding with PVP.

hydroxyl-carbonyl interactions. These trends are consistent with literature for interactions involving PVP and hydroxyl groups [47,48]. Further, the overlapping CH_2 stretching band (2950 cm^{-1}) is very weak in pure mangiferin, but it becomes more distinct with increasing PVP without any peak movement. The intensity of aromatic C=C stretching vibration (1615 cm^{-1}) gradually reduces due to the dilution effect, but this band also shows no spectral shift. Judging from the extent of C=O and O–H band shifts, the cross-hydrogen bonding of the PVP/mangiferin is more pronounced as compared to the PA/mangiferin. This preferential interaction of mangiferin to PVP relative to PA has resulted in macroscopic phase separation between the PA + mangiferin and PVP + mangiferin phases due to the partitioning (or screening) effect.

3.4. Miscibility characteristics of PA/PVP/mangiferin ternary blends

Varying extents of miscibility for the PA/PVP, PA/mangiferin, and PVP/mangiferin, there is no guarantee that the same miscibility trend will hold in their ternary case. The preferential affinity of mangiferin to PVP relative to PA can be manifested in the ternary blends of PA/PVP/mangiferin. Upon addition of mangiferin to the PVP rich-blends (e.g., 25/75 PA/PVP), a single glass transition is evident up to 80 wt% of mangiferin, but it becomes less distinct with further increase of mangiferin concentration due to the interference arising from the depressed melting point (Fig. 8(a)). However, in the case of 50/50 PA/PVP blends, the addition of only 10 wt% of mangiferin has led to liquid–liquid phase separation as manifested by the appearance of dual glass transition temperatures corresponding to those of PA + mangiferin and PVP + mangiferin compositions (Fig. 8(b)). It may be noted that the T_g's of the (PA + mangiferin) and (PVP + mangiferin) phases are 147 °C and 184 °C, respectively, which are higher than those of pure PA and PVP, i.e., 143 °C and 177 °C. This enhanced T_g's of these individual phases may be attributed to the higher glass transition temperature of mangiferin backbone, which is difficult to be detected by conventional DSC for the neat mangiferin due to the presence of the crystalline phase. Judging from the variation of the DSC scans with composition in Figs. 6(b) and 8(a), the T_g of the neat mangiferin, if it exists, might be located in the vicinity of 220 ± 10 °C that corresponds to the temperature range at which the T_g's of the high mangiferin concentrations appear to level off. It may be inferred that preferential interaction of mangiferin to PVP relative to PA probably has led to the liquid–liquid phase separation into the PVP + mangiferin and PA + mangiferin phases. This phase separated trend continues with further increase of mangiferin concentration in which the dual glass transitions shifted further to higher temperatures. At very high mangiferin loadings, these T_g transitions were interfered by the crystal melting peaks of mangiferin, implying a competition between liquid-liquid phase separation and crystal solidification. A similar competing trend of liquid–liquid phase separation with liquid–solid phase transition can be discerned in the PA rich-blend such as 75/25 PA/PVP (data not shown).

The phenomena of liquid–liquid phase separation and solid–liquid phase transition can be probed by an independent approach such as POM. The PA/mangiferin and PVP/mangiferin blends were transparent to naked eyes showing no indication of liquid–liquid phase separation at low mangiferin loading (Fig. 9). Further increase in mangiferin concentration resulted in crystallization of mangiferin exhibiting the large spherulitic structures in the continuum of isotropic liquid signifying the isotropic liquid + solid crystal coexistence phase. At very high concentrations of mangiferin, the entire field of optical microscope view was filled with truncated mangiferin spherulites. In the case of PA/PVP blends, the addition of mangiferin resulted in liquid–liquid phase separation due to the preferential interaction (or relative affinity) of mangiferin to PVP as compared to PA.

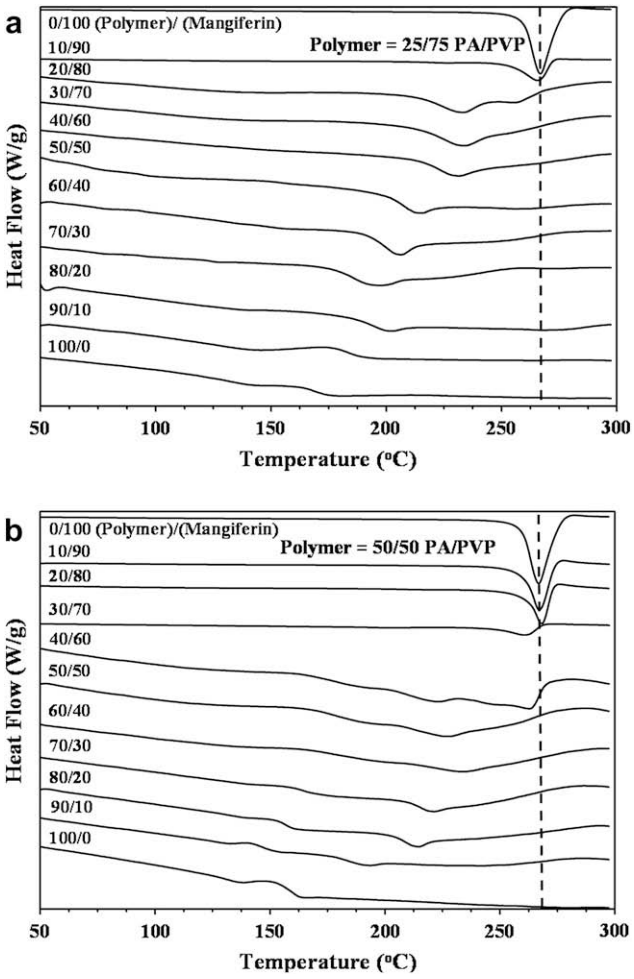

Fig. 8. Second run DSC thermograms for PA/PVP/mangiferin ternary blends with (a) 25/75 PA/PVP ratio exhibiting a single T_g shifting systematically to higher temperature with mangiferin loading and (b) 50/50 PA/PVP ratio showing liquid–liquid phase separation at lower mangiferin concentrations due to preferential affinity of mangiferin to PVP relative to PA. At higher mangiferin concentrations, crystallization of mangiferin takes place signifying liquid–solid phase transition.

To better appreciate this complex phase behavior, a ternary morphology phase diagram for PA/PVP/mangiferin ternary blends was mapped out based on information gathered from DSC along with the optical micrographs of the POM experiments (Fig. 9). Different types of shading were applied to delineate various coexistence regions. The symbols represent the data points obtained from the DSC experiments, showing a single phase (I) (open symbols), crystal solid (C) (filled symbols), two liquid coexistence phases (L + L) (half-filled), two liquid + crystal (I + C) regions, and the liquid + liquid + crystal solid phases (L + L + C) (hour glass-filled symbols). The phase boundaries of these coexistence regions were drawn by hand to guide the trend based on the morphology observation by POM. In the isotropic region indicated by 'I', the optical microscope picture (left middle) reveals uniformly transparent appearance but slightly tinted due to the inherent yellow color of mangiferin while the polarized condition shows complete darkness. These POM pictures are typical for a single phase mixture at the optical length scale, although it is not a proof. In the L + L biphasic region, bicontinuous morphology of a liquid–liquid phase separated region is evident in Fig. 9 (see upper left picture). This co-continuous

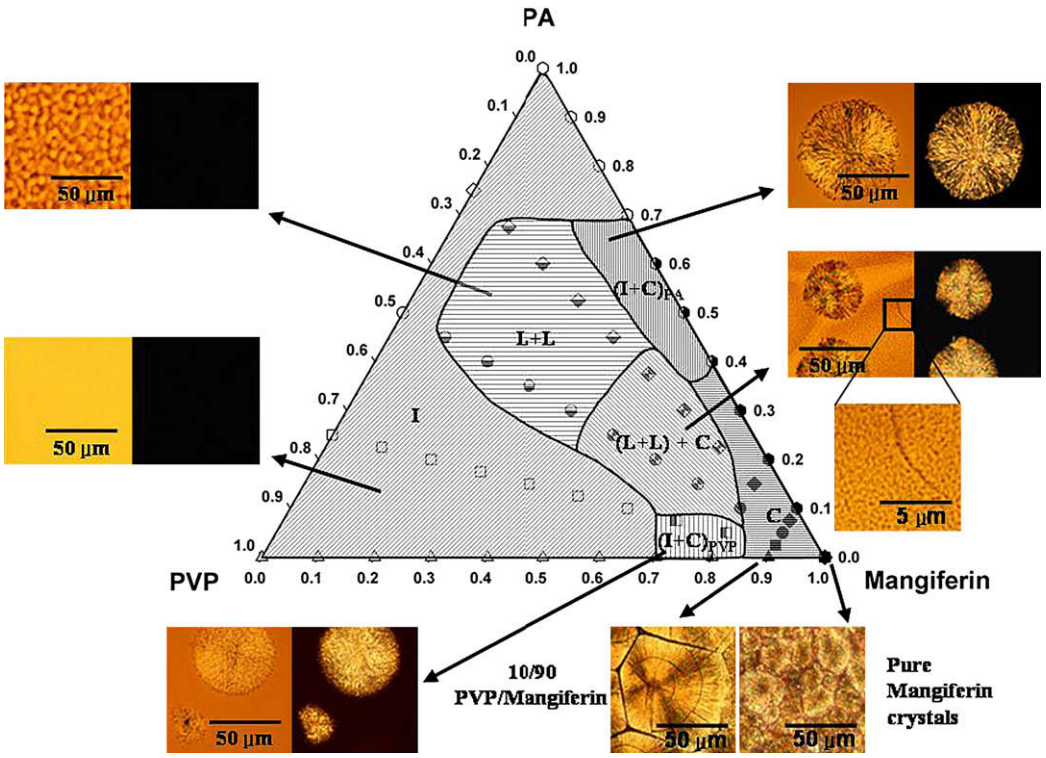

Fig. 9. Ternary morphology phase diagram, mapped out with the aid of POM and DSC data for the PA/PVP/mangiferin blends, showing various coexistence regions (labeled by different shading). Polarized and unpolarized of optical microscope images representing typical morphology of each region (except for the solid crystal region) are shown in relation to the ternary phase diagram. In the crystal region, the left image shows 10/90 PVP/mangiferin blend, whereas the right image shows that of the neat mangiferin crystals. Keys for labels are: I = isotropic (unfilled symbols), C = crystal (completely filled symbols), $(I+C)_{PVP}$ = coexistence of isotropic and crystals for PVP rich compositions (left-half-filled symbols), $(I+C)_{PA}$ = coexistence of isotropic and crystal for PA rich compositions (right-half-filled symbols), L + L = liquid + liquid (bottom-half-filled symbols), L + L + C = liquid + liquid + crystal (hour glass-filled symbols).

structure is a typical signature of spinodal decomposition, although by no means a proof. Further increase in mangiferin concentration resulted in crystallization of mangiferin showing the large spherulitic entities in the continuum of isotropic liquid signifying the isotropic liquid + crystal (I + C) coexistence phase (see the bottom left and the upper right pictures of Fig. 9). In the PA rich compositions and lower mangiferin concentrations, the lower solubility of mangiferin with PA has led to a larger $(I+C)_{PA}$ coexistence gap as compared to that of the $(I+C)_{PVP}$ region of the PVP/mangiferin. In the region marked by 'L + L + C', spherulitic (crystal) entities were found to be dispersed in a continuum of liquid–liquid phase separated matrix, which is in good agreement with the preceding DSC results. Finally, in the very high mangiferin contents, the whole field of view of POM is filled with truncated spherulitic crystals of mangiferin. Although the present ternary phase diagram involving the crystalline phase is complex, the crystallinity of mangiferin is capable of retaining its phytochemical properties relatively longer in drug delivery as compared with its isotropic amorphous counterpart. Thus the presence of mangiferin crystals in the polymer membranes may be advantageous for prolonged time release.

4. Conclusions

In summary, we have demonstrated the miscibility behavior of PA/PVP blend without and with mangiferin. The binary PA/PVP blends were completely miscible. The PA/mangiferin and PVP/mangiferin blends exhibited a single phase at low mangiferin loading, but large spherulites developed at higher mangiferin concentrations signifying the solid–liquid coexistence phase. The FTIR results revealed varying extents of cross-hydrogen bonding in the binary blends of PA/PVP, PA/mangiferin, and PVP/mangiferin, which are responsible for miscibility of these systems. Specifically, the blend miscibility is governed by the competition between the self-associating hydrogen bonding of the amide group of the PA molecules and the cross-hydrogen bonding between the N–H of PA and C=O of PVP. In high polymer blends the entropic driving force is extremely small and thus the attractive cross-hydrogen bonding must be stronger relative to that of the self-associating hydrogen bonding of PA in order to achieve a complete miscibility, especially like the present high polymer PA/PVP blends. In the ternary PA/PVP/mangiferin case, mangiferin has preferential cross-hydrogen bonding to PVP relative to PA. The addition of mangiferin to a completely miscible PA/PVP blends thus has led to liquid–liquid and liquid–solid phase separations in a manner dependent on composition as demonstrated in their ternary phase diagram. This phase separation phenomenon may be attributed to the partitioning effect of mangiferin caused by the greater affinity (i.e., cross-hydrogen bonding) of mangiferin to non-self-associating PVP relative to the self-associating PA. More importantly, the presence of mangiferin crystals is capable of retaining its phytochemical properties relatively longer in drug delivery as compared with its isotropic amorphous counterpart and therefore prolonged time release.

References

[1] Halliwell B. Lancet 1994;344(8924):721–4.
[2] Halliwell B. Annu Rev Nutr 1996;16:33–50.
[3] Gutteridge JM, Halliwell B. Ann NY Acad Sci 2000;899:136–47.
[4] Bolch A. J Am Diet Assoc 1995;95:493–6.
[5] Meskin MS, Bidlack WR, Davies AJ, Omaye ST. Phytochemicals in nutrition and health. Boca Raton, FL: CRC Press; 2002.
[6] Bao Y, Fenwick R. Phytochemicals in health and disease. Basel, NY: Marcel Dekker; 2004.

[7] Hench LL, Polak JM. Science 2002;295:1014–7.
[8] Ratner BD, Bryant SJ. Annu Rev Biomed Eng 2004;6:41–75.
[9] Matkar RA, Kyu T. J Phys Chem B 2006;110(32):16059–65.
[10] Dayal P, Matkar RA, Kyu T. J Chem Phys 2006;124(22):224902–7.
[11] Sanchez GM, Re L, Giuliani A, Nunez-Selles AJ, Davison GP, Leon-Fernandez OS. Pharmacol Res 2000;42:565–73.
[12] Muruganandan S, Gupta S, Kataria M, Gupta PK, Lal J. Toxicology 2005;176: 165–74.
[13] Garrido G, Delgado R, Lemus Y, Rodriguez J, Garcia D, Nunez-Selles AJ. Pharmacol Res 2004;50:165–72.
[14] Rodriguez J, Pierro DD, Gioia M, Monaco S, Delgado R, Coletta M, et al. Biochim Biophys Acta 2006;1760:1333–42.
[15] Andreu GP, Delgado R, Velho JA, Curti C, Vercesi AE. Eur J Pharm 2005;513:47–55.
[16] Leiro JM, Alvarez E, Arranz JA, Siso IG, Orallo F. Biochem Pharm 2003;65:1361–71.
[17] Guha S, Ghosal S, Chattopadhyay U. Chemotherapy 1996;42:443–5.
[18] Yoosook C, Bunyapraphatsara N, Boonyakiat Y, Kantasuk C. Phytomedicine 2000;6:411–9.
[19] Zheng MS, Lu ZY. Chinese Med J-Peking 1990;103:160–5.
[20] Zhu XM, Song JX, Huang ZZ, Wu YM, Yu MJ. Acta Pharmacol Sin 1993;14(5): 452–4.
[21] Stoilova I, Gargova S, Stoyanova A, Ho L. Herba Pol 2005;51(1–2):37–43.
[22] Garcia D, Leiro J, Delgado Sanmartin RML, Ubeira FM. Phytother Res 2003;17:1182–7.
[23] Leiro J, Arranz JA, Yanez M, Ubeira FM, Sanmartin M, Orallo LF. Int Immunopharmacol 2004;4:763–78.
[24] Sarkar A, Sreenivasan Y, Ramesh GT, Manna SK. J Biol Chem 2004;279:33768–81.
[25] Ichiki H, Miura T, Kubo M, Ishihara E, Komatsu Y, Tanigawa K, et al. Biol Pharm Bull 1998;21:1389–90.
[26] Miura T, Ichiki H, Hashimoto I, Iwamoto N, Kato M, Kubo M, et al. Phytomedicine 2001;8(2):85–7.
[27] Rajtar G, Zolkowska D, Kleinrok Z, Marona H. Acta Pol Pharm 1999;56(4):319–24.
[28] Lin CN, Hsieh HK, Liou SJ, Ko HH, Lin HC, Chung MI, et al. J Pharm Pharmacol 1996;48:887–90.
[29] Lin CN, Chung MI, Liou SJ, Lee TH, Wang JP. J Pharm Pharmacol 1996;48:532–8.
[30] Pinto MMM, Sousa ME, Nascimento MSJ. Curr Med Chem 2005;12:2517–38.
[31] Fotie J, Bohle DS. Anti-Infective Agents Med Chem 2006;5:15–31.
[32] Ghosal S, Biswas K, Chattopadhyay BK. Phytochemistry 1978;17(4):689–94.
[33] Schieber A, Berardini N, Carle R. J Agric Food Chem 2003;51:5006–11.
[34] Iseda S. Bull Chem Soc Jpn 1957;30(6):629–33.
[35] Nott PE, Roberts JC. Phytochemistry 1967;6:1597–9.
[36] Ellis TS. Macromolecules 1989;20(2):742–54.
[37] Ellis TS. J Appl Polym Sci 1988;36:451–66.
[38] Chen TI, Kyu T. Polym Commun 1990;21:111–4.
[39] Kyu T, Chen TI, Park H, White JL. J Appl Polym Sci 1989;37:201–13.
[40] Gohl H, Buck R, Strathmann H. Basic features of the polyamide membranes. In: Shaldon S, Koch KM, editors. Polyamide – the evolution of a synthetic membrane for renal therapy. Contrib Nephrol, 96; 1992. p. 1–25.
[41] Fox TG. Bull Am Phys Soc 1956;1:123.
[42] Coleman MM, Graf JF, Painter PC. Specific interactions and the miscibility of polymer blends. Lancaster, PA: Technomic Publ.; 1991.
[43] Painter PC, Coleman MM. Hydrogen bonding systems. In: Paul DR, Bucknall CB, editors. Polymer blends, vol. 1. Formulations. New York, NY: Wiley Interscience; 1999. p. 93.
[44] Taylor LS, Zografi G. J Pharm Sci 1998;87(12):1615–21.
[45] Buera MP, Levi G, Karel M. Biotechnol Prog 1992;8:144–8.
[46] Imamura K, Ohyama K, Yokoyama T, Maruyama Y, Imanaka H, Nakanishi K. J Pharm Sci 2008;97:519–28.
[47] Kuo SW, Chang FC. Macromolecules 2001;34:5224–8.
[48] Hu Y, Motzer HR, Etxeberria AM, Fernandez-Berridi MJ, Iruin JJ, Painter PC, et al. Macromol Chem Phys 2000;201:705–14.